NANO LETTERS

Letter

Cite This: Nano Lett. 2019, 19, 108−115

pubs.acs.org/NanoLett

Room-Temperature Strong Coupling of CdSe Nanoplatelets and Plasmonic Hole Arrays

Jan M. Winkler, Freddy T. Rabouw,† Aurelio A. Rossinelli, Sriharsha V. Jayanti, Kevin M. McPeak,‡ David K. Kim, Boris le Feber, Ferry Prins,§ and David J. Norris*

Optical Materials Engineering Laboratory, Department of Mechanical and Process Engineering, ETH Zurich, 8092 Zurich, Switzerland

Supporting Information

ABSTRACT: Exciton polaritons are hybrid light−matter quasiparticles that can serve as coherent light sources. Motivated by applications, room-temperature realization of polaritons requires narrow, excitonic transitions with large transition dipoles. Such transitions must then be strongly coupled to an electromagnetic mode confined in a small volume. While much work has explored polaritons in organic materials, semiconductor nanocrystals present an alternative excitonic system with enhanced photostability and spectral tunability. In particular, quasi-two-dimensional nanocrystals known as nanoplatelets (NPLs) exhibit intense, spectrally narrow excitonic transitions useful for polariton formation. Here, we place CdSe NPLs on silver hole arrays to demonstrate exciton−plasmon polaritons at room temperature. Angle-resolved reflection spectra reveal Rabi splittings up to 149 meV for the polariton states. We observe bright, polarized emission arising from the lowest polariton state. Furthermore, we assess the dependence of the Rabi splitting on the hole-array pitch and the number N of NPLs. While the pitch determines the in-plane momentum for which strong coupling is observed, it does not affect the size of the splitting. The Rabi splitting first increases with NPL film thickness before eventually saturating. Instead of the commonly used $\sqrt{N}$ dependence, we develop an analytical expression that includes the transverse confinement of the plasmon modes to describe the measured Rabi splitting as a function of NPL film thickness.

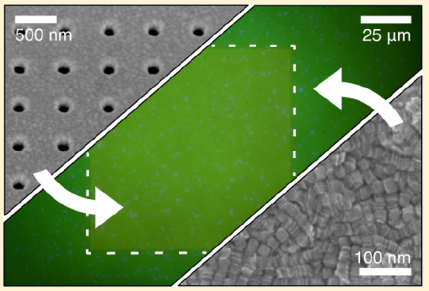

KEYWORDS: *Strong coupling, semiconductor nanoplatelets, plasmonic hole array, polariton emission, Rabi splitting, surface plasmons*

Coherent energy exchange between an electronic transition in matter and a resonant electromagnetic mode can result in the emergence of hybrid light−matter states known as polaritons.[1−6] When these polariton states have an energy separation, or Rabi splitting, that is larger than the line widths of the uncoupled light and matter states, the "strong coupling" regime is reached.[7−9] In other words, light−matter coupling is "strong" if energy is exchanged between light and matter on time scales faster than the dephasing of either component. To obtain strong coupling at room temperature, the Rabi splitting must exceed the temperature-induced broadening that electronic transitions typically exhibit.

Organic molecules coupled to surface plasmons have emerged as an excellent system for achieving strong coupling at room temperature.[10−14] When the localized electromagnetic fields of plasmons are combined with the large transition dipole moments of organic chromophores, the light−matter interactions can be sufficiently intense to observe strong coupling down to the single-molecule level.[15] If plasmonic surfaces such as metallic hole arrays are used to provide the field confinement, they also offer an open architecture, allowing convenient placement of electronic oscillators with easy optical and electronic access to excite and probe polaritons. Applications[16] as well as new phenomena, such as enhanced conductivity,[17] coherent emission,[18,19] polariton lasing,[20] and Bose−Einstein condensation,[21] have been reported for molecular systems strongly coupled to plasmonic modes.

However, the limited photostability and weak polariton−polariton interactions for strongly localized Frenkel excitons[22] can limit molecular systems. A more-photostable inorganic material with a large transition dipole can potentially provide an interesting alternative.[23−29] Ideally, such a material would also retain the advantageous properties of molecules such as solution-processability and scalability. To move in this direction, strong light−matter coupling at visible wavelengths using CdSe colloidal quantum dots[23−26] and in the near-infrared using single-walled carbon nanotubes[28,29] has been demonstrated.

Recently, quasi-two-dimensional semiconductor nanocrystals have been introduced that may provide even better performance for strong coupling.[30,31] These materials, referred to as nanoplatelets (NPLs), are rectangular-shaped particles

Received: August 23, 2018
Revised: November 30, 2018
Published: December 5, 2018

DOI: 10.1021/acs.nanolett.8b03422
Nano Lett. 2019, 19, 108−115

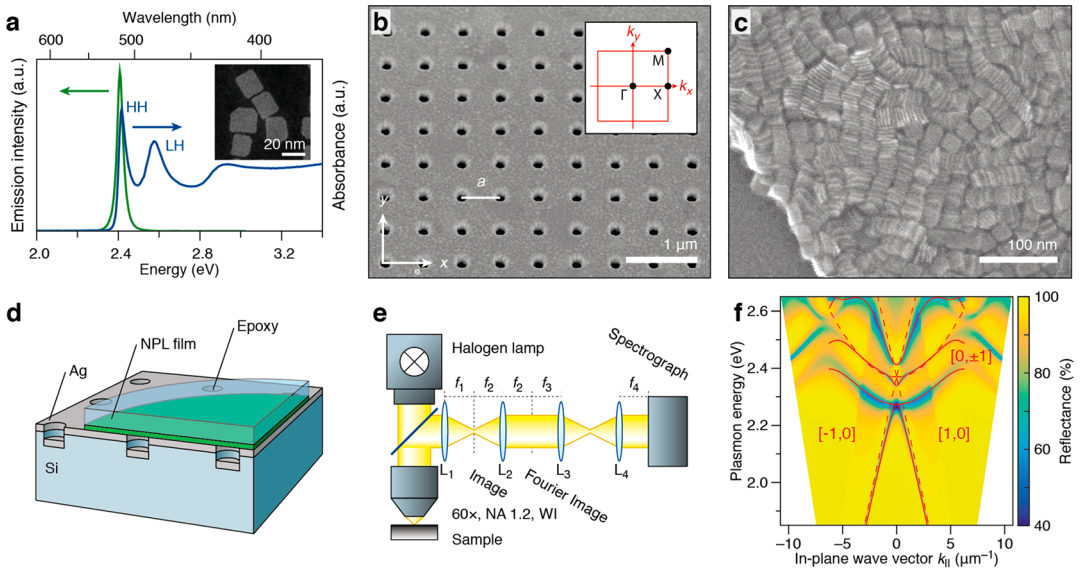

Figure 1. Components of our samples and their characterization. (a) Room-temperature absorption (blue) and emission (green) spectra of 4-monolayer CdSe NPLs dispersed in hexane. The absorption peaks at 513 (2.42) and 481 nm (2.58 eV) correspond to the HH and LH transitions, respectively. The inset shows a transmission electron micrograph of NPLs with lateral size of approximately 20 nm × 20 nm. (b) Scanning electron micrograph (SEM) of a bare Ag hole array with pitch a = 500 nm. The inset shows the first Brillouin zone of a square lattice. (c) SEM of a densely packed film of NPLs formed by drop casting a NPL dispersion onto an octadecyltrimethoxysilane-coated Si chip. The film edge is seen on the bottom left of the image. (d) The structure for investigating exciton−SPP interactions, consisting of a film of NPLs attached to a backing layer of epoxy and placed on top of a Ag hole array. (e) The Fourier imaging set up used to obtain the momentum-resolved reflection spectra that reveal the dispersion of our hole arrays. The lenses L_i with focal length f_i (see the Supporting Information) project the Fourier image onto the entrance slit of the spectrograph. (f) The experimental plasmonic band structure of a bare Ag square hole array with a = 500 nm. The theoretical hole-array dispersion without SPP−SPP coupling (eq 1; dashed red line) and with SPP−SPP coupling (red solid line; see the Supporting Information for details) are shown for comparison.

that are tens of nanometers on a side but only a few atomic layers thick. Moreover, samples can be synthesized in which all NPLs have the same thickness (e.g., four monolayers). Because this precisely defined dimension determines the excitonic energies, the inhomogeneous broadening present in the optical transitions of quantum dots is significantly reduced for NPLs. The resulting narrow transition line widths combined with large absorption cross-sections[32,33] make NPLs an intriguing material for light−matter coupling with the potential to achieve high values for the "cooperativity" parameter, which quantifies the coupling strength between light and matter states relative to their line widths. Indeed, strong coupling of NPLs to optical modes in a micrometer-scale Fabry−Pérot cavity has already been shown.[34] However, the potential of these colloidal nanoparticles for plasmonic strong coupling remains unexplored.

Here, we present strong coupling of CdSe NPLs to surface plasmon polariton (SPP) modes on a Ag hole array. Reflection spectra reveal three polariton states, which arise due to the coupling of the dispersive SPP mode with the two lowest-energy excitonic transitions in the NPLs. We observe Rabi splittings up to 149 meV, which is 2.3 times larger than those previously measured for NPLs in an optical cavity.[34] The larger splittings arise because here the emitters sit in the electric field maximum of the SPP mode. In our open resonator design, this plasmon mode occurs at the surface of the hole array and is, therefore, easily accessible for placing, exciting, and probing emitters. We also examine the dependence of the Rabi splitting, $\hbar\Omega_R$, on the thickness of the NPL film. While the splitting in previous works (with films of electronic oscillators thinner than 100 nm) scaled as $\sqrt{d}$, where d is the thickness of the film,[23,35] we confirm here a theoretical prediction[36] that the splitting saturates as the film thickness extends beyond the exponentially decaying plasmon field. Our findings highlight the potential of NPLs for strong coupling and provide general guidance for optimizing light−matter coupling in evanescent fields.

The components of our samples are shown in Figure 1. We synthesized four-monolayer-thick zincblende CdSe NPLs[37] (see the transmission electron micrograph in the inset of Figure 1a). These NPLs exhibit two distinct absorption peaks in the visible at 513 (2.42) and 481 nm (2.58 eV), which correspond to the heavy-hole (HH) and light-hole (LH) transitions, respectively (Figure 1a).[31] Both have large transition dipoles, as reflected by their large absorption cross-sections.[33] The band-edge HH transition emits with a quantum yield reported to be up to 50% (see Figure 1a for spectrum).[31] In absorption (emission), the HH feature exhibits line widths as narrow as 36 (34 meV), which is narrower than state-of-the-art quantum dots (ensemble emission line widths of 67 meV)[38] due to reduced inhomogeneous broadening and weak phonon coupling in NPLs.

We then prepared plasmonic hole arrays[39] by fast thermal evaporation[40] of Ag onto a Si substrate prepatterned with a square array of holes (see the Supporting Information for details). The scanning electron micrograph (SEM) in Figure 1b shows a close-up of the resulting 100 μm × 100 μm Ag hole array with a lattice spacing (pitch) of a = 500 nm.

To study exciton−SPP interactions, we must place the NPLs directly on top of this Ag hole array, where the SPP electric-field intensity is high. For this, we exploited nanocrystal template stripping.[41] We first drop-cast NPLs from a 9:1 mixture of hexane to octane onto a flat Si chip coated with an

DOI: 10.1021/acs.nanolett.8b03422
Nano Lett. 2019, 19, 108−115

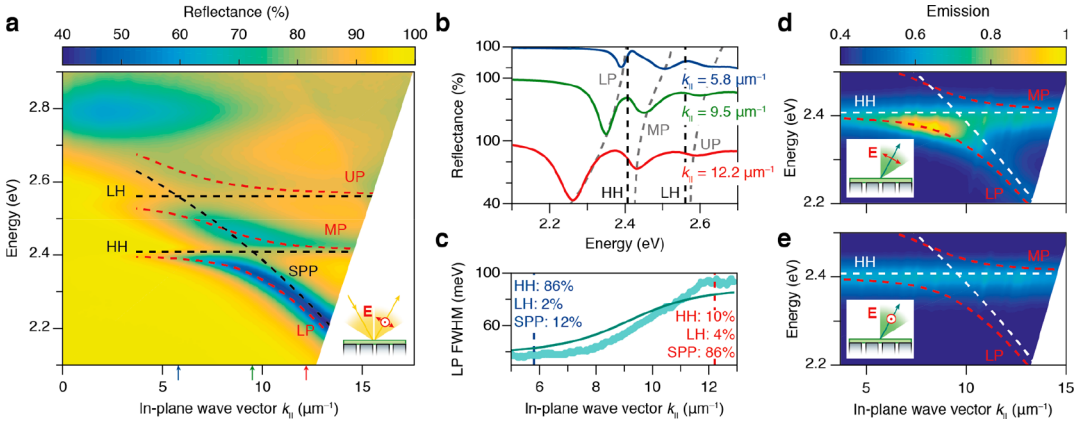

Figure 2. Angle-resolved spectroscopy of CdSe-NPL-covered Ag hole arrays at room temperature. (a) Angle-resolved reflection spectrum of a 79 nm thick NPL film deposited on a square Ag hole array with pitch a = 180 nm. A total of three separate polariton branches [lower (LP), middle (MP), and upper polariton (UP); red dashed lines] arise from the interaction between the dispersed plasmonic band and the exciton transitions of the NPLs (SPP, HH, and LH; black dashed lines). The Rabi splittings for this structure are 110 and 139 meV at the HH and LH transitions, respectively. (b) Cross-sections through the reflectance map (shown in panel a) at selected values of $k_{\parallel}$. The gray dashed lines provide a guide to the eye for the evolution of the polariton branches. (c) Line width of the LP branch as a function of $k_{\parallel}$. The insets indicate the composition of the LP at $k_{\parallel}$ = 5.8 and 12.2 μm^{-1} based on the coupled-mode model (see the Supporting Information for details). (d) Emission from the LP state adopts the transverse-magnetic polarization of the plasmon band to which the excitonic transition is strongly coupled. (e) When we analyze the emission with transverse-electric polarization we observe only band-edge emission at 2.4 eV from uncoupled NPLs. The insets indicate the alignment of the polarizer placed in front of the spectrograph.

octadecyltrichlorosilane self-assembled monolayer.[42] The thickness of the NPL film was controlled by varying the NPL concentration in the liquid dispersion while maintaining the drop-cast volume and the Si chip size. Figure 1c shows a film of NPLs that resulted from this process. We note that it contains local ordering of the NPLs into "stacklets." Separate stacklets then appear to be relatively randomly oriented. Such NPL films were then "stripped off" the Si using ultraviolet-light-curable epoxy.[41] The ultrasmooth surface previously in contact with the Si was placed via van der Waals bonding onto the Ag hole array. This yields the epoxy/NPL/Ag-hole-array structure depicted schematically in Figure 1d.

Such samples can then be characterized on an optical microscope. The periodic structure of the Ag hole array provides in-plane momentum to incident photons. SPPs with wave vector $\vec{k}_{SPP}$ are then launched on the metal surface when:

$$|\vec{k}_{\parallel} + i\vec{G}_x + j\vec{G}_y| = |\vec{k}_{SPP}| = \frac{\omega}{c}\sqrt{\frac{\varepsilon_m(\omega)\varepsilon_d(\omega)}{\varepsilon_m(\omega) + \varepsilon_d(\omega)}} \quad (1)$$

where $\vec{k}_{\parallel}$ is the in-plane wave-vector component of the incident photon, $\vec{G}_x = (2\pi/a, 0)$ and $\vec{G}_y = (0, 2\pi/a)$ are the reciprocal lattice vectors of the square periodic structure, and i and j = 0, ±1, ±2,... are integers. In eq 1, $\varepsilon_m(\omega)$ and $\varepsilon_d(\omega)$ are the frequency-dependent dielectric functions of the Ag and the dielectric material above it, respectively.

The plasmonic hole-array dispersion represented by eq 1 is experimentally measured using the Fourier imaging setup[19,43] shown in Figure 1e. White light is reflected off the sample, and the Fourier image is then projected onto the entrance slit of an imaging spectrograph. Here we focus on the dispersion along the Γ−X direction in reciprocal space (see Figure 1b, inset). Thus, we align the entrance slit of the spectrograph along the x direction of the hole array to probe the plasmonic dispersion using incident photons of wave vector $\vec{k}_{\parallel} = (k_0 \sin\theta, 0)$ where k_0 is the wave-vector magnitude and θ is the angle of incidence with respect to the surface normal.

Figure 1f shows the in-plane-momentum-resolved reflection spectrum of a bare Ag square hole array (i.e., with air instead of NPLs as the dielectric medium) with a lattice spacing of a = 500 nm. Points of low reflectance in the plot indicate successful coupling of photons to SPPs for the corresponding momentum and energy values. The two linear branches in the dispersion relation between 1.8 and 2.4 eV labeled [±1, 0] result from photons coupled to SPPs with array contributions of $\pm 1\vec{G}_x$. These branches show line widths down to 30 meV thanks to the high quality of the plasmonic hole array (see Figure S3 for cross-sections of Figure 1f). The flatter, parabolic features near 2.4 eV, labeled [0, ±1], are due to contributions $\pm 1\vec{G}_y$. The plasmonic hole-array dispersion according to eq 1 is overlapped as red dashed lines. The discrepancies between eq 1 and the measurements at $\vec{k}_{\parallel} = 0$ (Γ point) and along the theoretically degenerate [0, ±1] branches result from SPP−SPP interactions.[39,44,45] When these are included, the degeneracy of the [0, ±1] branches is lifted and an energy gap opens at $k_{\parallel} = 0$ (see the Supporting Information for details on the coupled-mode model).[46] The energetic position of this gap can be tuned by changing the lattice spacing a of the hole array and thus modifying the reciprocal lattice vectors $\vec{G}_x$ and $\vec{G}_y$.

Now that we understand the dispersion diagram for our bare Ag hole arrays, we turn to those with NPLs. Figure 2a shows a typical example for a Ag hole array with a = 180 nm and a 79 nm thick layer of CdSe NPLs (reflectance maps of hole arrays with different NPL layer thicknesses are shown in Figure S6). Clear anticrossings are observed between the HH and LH excitonic transitions of the NPLs (which would be present as horizontal lines in such a plot without coupling to plasmons) and the plasmonic [±1, 0] band (SPP). The exciton−SPP interaction leads to the formation of three energetically separated polariton branches: a lower polariton (LP) branch between 2.20 and 2.41 eV, a middle polariton (MP) branch between 2.41 and 2.56 eV, and an upper polariton (UP) branch between 2.56 and 2.70 eV. Using a coupled-mode model for the polariton states (red dashed lines; see the

DOI: 10.1021/acs.nanolett.8b03422
Nano Lett. 2019, 19, 108−115

Supporting Information) we can extract the light−matter interaction strength g. From this, we can calculate Rabi splittings $\hbar\Omega_R = 2g$ of 110 and 139 meV for the HH and the LH transitions, respectively. This indicates that our system is well into the strong-coupling regime, as the splitting is larger than the line widths of the SPP (γ_{SPP} = 32 meV; [1, 0] branch in Figure 1f at $k_{||} = 1\ \mu m^{-1}$) and the exciton (γ_{HH} = 36 meV).[8] Based on these values we calculate a cooperativity $C = 4g^2/(\gamma_{SPP}\gamma_{HH})$ of 10.5 for the HH−SPP coupling. (We will, however, show and discuss below that the Ag−NPL SPP is more lossy than the Ag−air SPP, translating into a reduced cooperativity of C = 3.7 for the coupled system.) Furthermore, the time scale associated with exciton−SPP energy exchange of $1/\Omega_R \approx 10^{-13}$ s is considerably faster than those reported for Förster resonance energy transfer between NPLs in stacks (down to 10^{-11} s; see refs 47 and 48). The here-measured Rabi splittings and cooperativity values are larger than those observed for spherical CdSe nanocrystals coupled to propagating SPPs on thin Ag films (112 meV; $C \approx 2$; ref 23) and for CdSe NPLs in an optical Fabry−Pérot cavity (66 and 58 meV for the HH and the LH transitions, respectively; $C \approx 3.4$; ref 34). The work by Wang et al.[25] reported a Rabi splitting of 220 meV for spherical nanocrystals placed on a Au hole array. However, the broader absorption line width (160 meV) of their CdSe quantum dots leads to cooperativity values down to $C \approx 1.9$.

To analyze the polariton line widths, we consider cross-sections through the reflectance map of Figure 2a at fixed values of $k_{||}$. Figure 2b shows three examples of resulting reflection spectra, taken at $k_{||} = 5.8\ \mu m^{-1}$ (blue), where the bare SPP is resonant with the LH exciton; $k_{||} = 9.5\ \mu m^{-1}$ (green), where the bare SPP is resonant with the HH exciton; and $k_{||} = 12.2\ \mu m^{-1}$ (red), where the bare SPP is red detuned from both excitons. The line width of each polariton branch (LP, MP, and UP) seems to depend on $k_{||}$. The dependence is most apparent and can be best quantified for the pronounced LP reflectance dip. Figure 2c shows the LP line width as a function of $k_{||}$. The line width is narrow at low $k_{||}$, where the LP is mainly excitonic, and increases toward higher $k_{||}$, where the LP becomes more plasmonic. The data can be described by a model (solid line in Figure 2c) in which the LP line width is the weighted average of the line widths of the uncoupled HH, LH, and SPP components. The momentum-dependent weighting factors (also called Hopfield coefficients) are given by the coupled-mode model (see the Supporting Information for details). We assume that the uncoupled HH and LH line widths are the same as for NPLs in a liquid dispersion (see Figure 1a) and use the uncoupled SPP line width as the only free parameter. From a fit of the model to the data, we obtain a value of 90 meV for this parameter, which is larger by a factor 2.8 compared to the SPP line width we measured in Figure 1f for the Ag−air interface. We ascribe the broader SPP line width of our Ag−NPL sample to two effects. First, the higher refractive index of NPLs compared to air increases SPP losses as it increases the fraction of plasmon field inside the Ag, which is lossy. Second, the hole-array pitch for our Ag−NPL is smaller, which corresponds to a higher surface density of outscatterers, resulting in increased SPP losses. Considering the revised SPP line width, the cooperativity value of our system is C = 3.7.

Because our NPLs are also fluorescent, we can investigate the emission properties of the polaritons. We excite the same strongly coupled NPL−SPP system with a 385 nm light-emitting diode and measure the momentum-resolved photoluminescence with a transverse-magnetic (TM; polarizer aligned along the spectrograph slit) or a transverse-electric (TE; polarizer aligned perpendicular to the slit) polarizer, respectively (Figure 2d,e). Photoluminescence from the LP branch is observed only under TM polarization (Figure 2d). Indeed, hybridization of excitons and plasmons leads to polarization of the initially nonpolarized photoluminescence.[28,49] In addition to emission from the strongly coupled LP state, we observe undispersed band-edge emission from uncoupled NPLs at 2.4 eV that is independent of polarizer orientation (Figure 2d,e). This uncoupled emission was not visible in previous experiments measuring strong coupling of NPLs in a Fabry−Pérot resonator[34] because only emission into cavity modes was collected.

By changing the pitch of the hole array, we can tune the wave vector value at which the exciton transitions are resonant with the plasmonic bands (eq 1). This is commonly used to bring the light−matter anticrossing to $k_{||} = 0$ (Γ point) so it can be probed at normal incidence.[17,25] For the structure presented in Figure 2a, light at normal incidence would be resonant with the HH exciton for a hole spacing of ∼230 nm. However, it is important to realize that for other array periodicities strong coupling will still occur, just at other values of $k_{||}$.[11] It remains an open question whether the strength of the light−matter interaction is influenced by where in the Brillouin zone the exciton−SPP anticrossing occurs.[8] To probe this question, we compare the polariton dispersion measurements of a 79 nm thick film of NPLs coupled to SPPs on square hole arrays with different pitches a. In each case, we set the diameter of the holes to $a/4$. Figure 3a plots the resulting polariton dispersion curves reconstructed from the angle-resolved reflection spectra (cf. Figure 2a) by adding the corresponding grating momentum for each pitch (see equations in the inset of Figure 3a, section S4, and Figure S4). Interestingly, the data points originating from hole arrays of different pitch (different colors in Figure 3a) collapse onto the same exciton polariton dispersion relation. We conclude that, for the range of lattice parameters considered, the hole array does not affect the SPP dispersion nor the strong coupling. It simply provides in-plane momentum that allows us to probe the polariton dispersion outside the light cone. The Rabi splittings, reflecting the strength of exciton−SPP coupling, are independent of $k_{||}$ over the range ($2-10\ \mu m^{-1}$) probed by our experiments. For larger pitches (a > 220 nm) the splitting would occur closer to $k_{||} = 0$ (Γ point), where multiple SPP bands are degenerate. While this is the situation in many previous experiments,[25] the interplay between SPP−SPP interactions[46] and exciton−SPP coupling makes the analysis complicated. We intentionally avoid these complexities by considering only coupling at large $k_{||}$ values, so that we can reconstruct the fundamental exciton polariton dispersion relation of the strongly coupled system from reflection data by simply adding momentum. Polariton dispersion relations presented below are similarly obtained by averaging multiple measurements on hole arrays with different pitch but with NPL films of the same thickness.

A common approach to modify the light−matter coupling constant g is to change the number of electronic oscillators N coupled to an electromagnetic mode, as $g \propto \sqrt{N/V}$ where V is the modal volume.[19,23,28] For studies using molecules, this can be done by changing the molecular concentration in a polymer

DOI: 10.1021/acs.nanolett.8b03422
Nano Lett. 2019, 19, 108−115

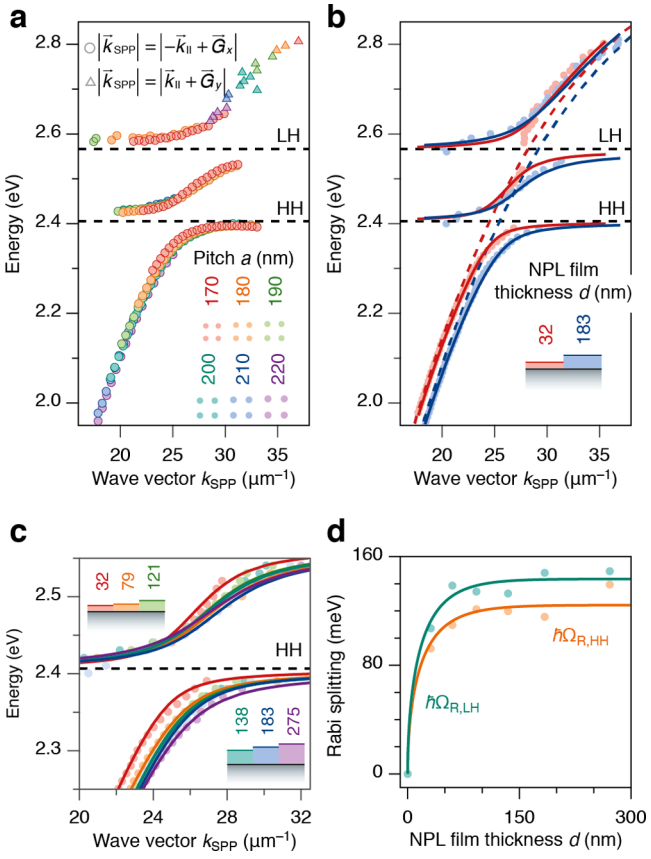

Figure 3. Exciton polariton dispersion diagrams as a function of hole-array pitch and NPL film thickness. (a) The polariton dispersion of SPPs coupled to the HH and LH transitions in CdSe NPLs reconstructed by adding the corresponding grating momentum to reflection measurements (e.g., as in Figure 2a) obtained from hole arrays with various pitches (different colors). Momentum is included from the *x* direction (circles) or the *y* direction (triangles). (b) A coupled-mode model fits the polariton dispersion curves obtained from hole arrays with 32 (red) and 183 nm thick (blue) films of CdSe NPLs. (c) A close-up of the HH transition reveals that the polariton dispersion depends on NPL film thickness but saturates beyond ∼100 nm. (d) The experimental Rabi splittings for the HH (orange line) and LH (green line) transitions first increase but then saturate for NPL films thicker than ∼100 nm.

matrix that is then placed in the mode.[19,20] For our experiments, we use densely packed NPL films. Thus, we vary *N* via the film thickness. Indeed, previous studies of strong coupling between films of electronic oscillators and plasmon modes have found a square-root dependence of the coupling constant *g* on the film thickness.[23,28,35] However, the intensity of SPP modes decays exponentially away from the metal−dielectric interface with a transverse confinement length of ∼100 nm at visible wavelengths.[50] Thus, after an initial square-root dependence, increasing the film thickness beyond the transverse SPP confinement length should not further enhance *g* because additional electronic oscillators no longer couple to the SPP mode. This saturation effect has been discussed theoretically.[36] We study it here experimentally on NPL layers up to a thickness of 275 nm (see Figure S6 for the corresponding reflectance measurements). Figure 3b shows the polariton dispersion relation of SPPs strongly coupled to NPL films that are 32 (red circles) and 183 nm (blue circles) thick. The red and blue solid lines present a fit to the data using the coupled-mode model. Upon increasing the layer thickness, the HH−SPP Rabi splitting increases from 92 to 116 meV and the LH−SPP Rabi splitting from 107 to 148 meV. Figure 3c shows the polariton dispersions close to the HH transition for the complete series of measured NPL film thicknesses. From these measurements, we can extract the HH−SPP and LH−SPP coupling constants g_{HH} and g_{LH} as a function of the NPL layer thickness *d* (Figure 3d and Table S1). We see that the coupling constants initially increase with *d* and then, as expected, approach a constant value for thicker films. The maximum Rabi splittings ($\hbar\Omega_R = 2g$) obtained are 139 and 149 meV for the HH and LH transitions, respectively.

The coupled-mode model offers a convenient empirical way to describe the experimental polariton splitting in terms of the coupling constant *g*. However, it does not explicitly consider the finite extension of the SPP field into the NPL layer and, hence, does not provide insight into the observed saturation of the Rabi splitting for thick NPL films. For this, we used an alternative classical model to describe strong coupling, starting from the SPP dispersion relation (eq 1) and including excitonic transitions of the NPLs as Lorentz terms in the dielectric function $\varepsilon_d(\omega)$.[8] Figure 4a shows a schematic of the three-layer geometry used in our experiments. The optically thick Ag film is covered with a NPL layer of thickness *d* followed by a semi-infinite slab of epoxy. A complex refractive index can be assigned to each layer and the dispersion relation for electromagnetic modes bound to the Ag−NPL interface can be evaluated by solving Maxwell's equations with the appropriate boundary conditions.[51] To simplify the calculations, we approximated the NPL and epoxy layer as a single effective medium (Figure 4b) with a refractive index that is the weighted average for the NPL and the epoxy:

$$n_{eff}(d) = f(d)n_{NPL} + [1 - f(d)]n_{epoxy} \quad (2)$$

$$f = \frac{\int_0^d e^{-z/\delta_{SPP,z}}dz}{\int_0^\infty e^{-z/\delta_{SPP,z}}dz} = 1 - e^{-d/\delta_{SPP,z}} \quad (3)$$

The weighting factor *f* is the fraction of the SPP field intensity inside the NPL film with thickness *d*, where $\delta_{SPP,z}$ is the transverse SPP confinement length assuming Ag covered with a semi-infinite slab of NPLs (see the Supporting Information for details on the linear-dispersion model). The frequency-dependent refractive index of the NPL layer $n_{NPL}(\omega)$ was modeled by using Cauchy's equation to define a transparent background with two added Lorentzian oscillators representing the HH (including potential nearby higher-energy states)[52] and LH transitions.[53] A second Cauchy's equation was employed for the refractive index $n_{epoxy}(\omega)$ of the epoxy layer, and the refractive index of Ag was taken from the literature.[40] The parameters describing $n_{epoxy}(\omega)$ were determined by fitting eq 1 with $\varepsilon_d(\omega) = n_{eff}^2(\omega,d = 0) = n_{epoxy}^2(\omega)$ to the SPP dispersion relation reconstructed from hole arrays covered with only epoxy (see gray points in Figure 4c). Subsequently, a single set of parameters describing $n_{NPL}(\omega)$ (see Figure 4f) was determined from simultaneously fitting SPP dispersion relations (eq 1) with $\varepsilon_d(\omega) = n_{eff}^2(\omega,d)$ to the polariton dispersion relations of hole arrays covered with NPL layers of six different thicknesses *d*. The NPL film thicknesses were fixed parameters in the model optimization, as determined using atomic force microscopy (AFM). (Additional details for the model and the AFM measurements

DOI: 10.1021/acs.nanolett.8b03422
Nano Lett. 2019, 19, 108−115

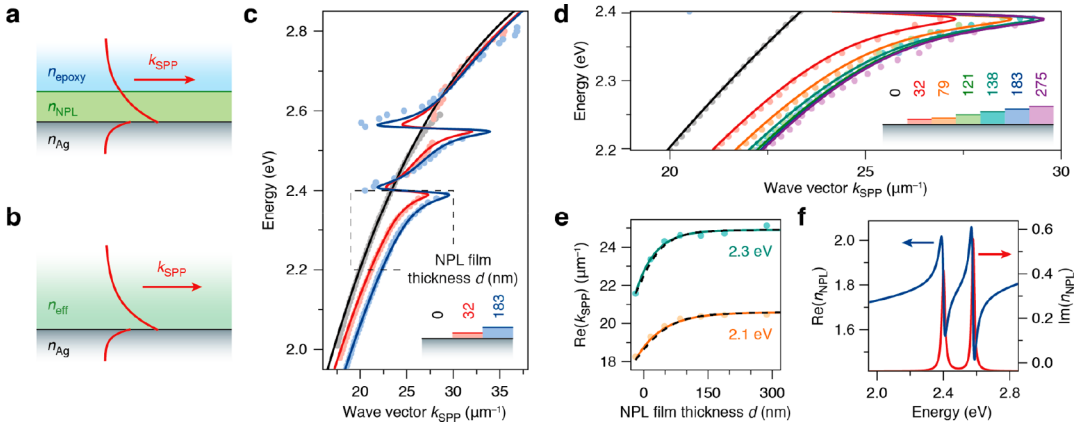

Figure 4. Modeling of strong coupling for CdSe NPL films on Ag hole arrays. (a) Our experimental geometry consists of a Ag film covered with a NPL film of thickness d that is backed by a layer of epoxy. (b) Assuming an effective refractive index composed of a linear combination of the NPL and the epoxy refractive indices yields a simple analytical expression for the SPP dispersion. (c) With a single set of parameters, the effective refractive index model (solid lines) captures the experimental SPP dispersion (data points) for a vanishing NPL film (black) as well as the polariton dispersions for NPL films that are 32 (blue) and 183 nm (red) thick. (d) The polariton dispersion at energies slightly red-shifted from the HH transition (dashed box shown in panel c). The polariton wave vector first increases as the NPL film becomes thicker but then saturates for thicker NPL films. (e) The dependence of polariton wave vector on NPL film thickness at an energy far from the HH transition (2.1 eV; orange) and close (2.3 eV; green). Solid colored lines represent the theoretical wave vectors according to the effective-index model (shown in panel b); black dashed lines are those calculated by explicitly considering the three-layer geometry (shown in panel a).[51] (f) The refractive index of the NPL film, modeled by a sum of two Lorentzian oscillators and a Cauchy background with parameters optimized by globally fitting the polariton dispersion curves for all NPL film thicknesses (see the Supporting Information).

are given in the Supporting Information.) The results of the global fit are shown in Figure 4c–e. The experimental dispersion relations (data points) and the corresponding fits (lines) for two film thicknesses (red, 32 nm; blue, 183 nm) are plotted in Figure 4c. The complete set of NPL film thicknesses is shown for the energy range just below the HH transition in Figure 4d. We see that the model based on an effective medium is able to reproduce the experimental dispersion for all layer thicknesses with a single set of parameters describing the refractive index of the NPL layer (see Table S2). Figure 4e shows the real part of the polariton wave vector at 2.1 and 2.3 eV as a function of film thickness. Initially, the polariton wave vector becomes larger for increasing NPL film thickness but then saturates when the thickness exceeds the transverse SPP confinement length (55 nm at 2.1 eV and 40 nm at 2.3 eV). Solid lines in Figure 4e denote the thickness-dependent wave vector according to our simplified Lorentz model using an effective refractive index, matching the experimental data. Our effective-index model is also in good agreement with mode calculations that take into account the three-layer geometry explicitly (dashed lines Figure 4e).[51]

The frequency-dependent refractive index of the NPLs obtained from the Lorentz model is plotted in Figure 4f. Comparing the imaginary part of n_{NPL} (red line in Figure 4f) with the absorption spectrum of the NPLs (Figure 1a), we see that the energies of the HH and LH peaks agree well. However, our model of two Lorentzian absorption lines does not quantitatively reproduce the absorption spectrum of the NPLs, which consists of many transitions spanning from green (2.4 eV) to ultraviolet wavelengths.

Finally, we can use the results of the simple Lorentz model to quantify the saturation behavior of the Rabi splittings, $\hbar\Omega_{R,HH} = 2g_{HH}$ and $\hbar\Omega_{R,LH} = 2g_{LH}$, with increasing NPL film thickness (Figure 3d). We adapt the well-known relation[8] $g \propto \sqrt{N/V}$ to the situation of a plasmon mode that decays exponentially into a densely packed film of emitters. An expression for g as a function of the film thickness d is obtained by weighing the constant number density of NPLs inside the emitter film N/V with the overlapping plasmon field intensity:[36]

$$g(d) \propto \frac{1}{n_{eff}(d)}\sqrt{\frac{N}{V}(1 - e^{-d/\delta_{SPP,z}})} \quad (4)$$

Here, the factor $1/n_{eff}$ (eq 2) takes into account that the electric-field intensity of an optical mode scales inversely with the refractive index squared of the medium.[54] Eq 4 approaches a constant saturation value of $\sqrt{N/V}/n_{NPL}$ in the limit of large film thicknesses. Alternatively, we retrieve in first order the $g \propto \sqrt{d}$ dependence observed previously for systems using thin films of electronic oscillators[23,35] by expanding eq 4 as a series around $d = 0$. The full expression accurately reproduces the saturation behavior of g in our experiments (Figure 3d).

In summary, we have demonstrated strong coupling between SPPs supported on a Ag hole array and CdSe NPLs. Using momentum-resolved reflection spectroscopy, we measured Rabi splittings of up to 139 and 149 meV for SPP coupling to the heavy- and light-hole transitions of the NPLs, respectively. The magnitude of the splitting could potentially be further increased by aligning the in-plane-oriented heavy-hole exciton of the NPLs[55] with the transverse magnetic SPP field using recently developed self-assembly techniques.[56] Further, the Rabi splitting is independent of the pitch of the hole array, at least as long as the splitting occurs away from $k_{\parallel} = 0$ (Γ point). The influence of plasmonic energy gaps near the Γ point and their associated high density of optical states on strong coupling remains unclear. Finally, by examining samples with different NPL film thicknesses, we demonstrated saturation of the light–matter coupling strength as the NPL film thickness exceeds the transverse SPP confinement length. Our results highlight CdSe NPLs as a promising material to achieve strong light–matter coupling. Moreover, they provide

DOI: 10.1021/acs.nanolett.8b03422
Nano Lett. 2019, 19, 108–115

important insights into the effects of sample geometry on the strength of SPP−matter coupling.

■ ASSOCIATED CONTENT

Supporting Information

The Supporting Information is available free of charge on the ACS Publications website at DOI: 10.1021/acs.nanolett.8b03422.

Figures, tables, and text including a description of the sample fabrication and the optical setup, AFM data on the NPL film thickness measurements, and additional details of the coupled-mode model and the linear-dispersion model (PDF)

■ AUTHOR INFORMATION

Corresponding Author

*E-mail: dnorris@ethz.ch.

ORCID

Jan M. Winkler: 0000-0001-5062-8523
Freddy T. Rabouw: 0000-0002-4775-0859
Aurelio A. Rossinelli: 0000-0001-6930-4190
Kevin M. McPeak: 0000-0002-2766-104X
Ferry Prins: 0000-0001-7605-1566
David J. Norris: 0000-0002-3765-0678

Present Addresses

[†]Debye Institute for Nanomaterials Science, Utrecht University, Princetonplein 1, 3584 CC Utrecht, The Netherlands
[‡]Cain Department of Chemical Engineering, 3315L Patrick F. Taylor Hall, Louisiana State University, Baton Rouge, LA 70803, United States
[§]Condensed Matter Physics Center (IFIMAC), Universidad Autónoma de Madrid, 28049 Madrid, Spain

Funding

This work was supported by the Swiss National Science Foundation under award no. 200021-165559 and the European Research Council under the European Union's Seventh Framework Program (FP/2007−2013)/ERC grant agreement no. 339905 (QuaDoPS Advanced Grant). B.l.F. and F.T.R. acknowledge support from The Netherlands Organization for Scientific Research (NWO, Rubicon grant nos. 680-50-1513 and 680-50-1509, respectively). F.P. thanks the Swiss National Science Foundation under the Ambizione Program.

Notes

The authors declare no competing financial interest.

■ ACKNOWLEDGMENTS

We thank F. A. Antolinez and J. Cui for stimulating discussions and U. Drechsler, S. Meyer, A. Olziersky, and H. Rojo for technical assistance.

■ REFERENCES

(1) Skolnick, M. S.; Fisher, T. A.; Whittaker, D. M. *Semicond. Sci. Technol.* **1998**, *13*, 645−669.
(2) Khitrova, G.; Gibbs, H. M.; Jahnke, F.; Kira, M.; Koch, S. W. *Rev. Mod. Phys.* **1999**, *71*, 1591−1639.
(3) Khitrova, G.; Gibbs, H. M.; Kira, M.; Koch, S. W.; Scherer, A. *Nat. Phys.* **2006**, *2*, 81−90.
(4) Reithmaier, J. P. *Semicond. Sci. Technol.* **2008**, *23*, 123001.
(5) Deng, H.; Haug, H.; Yamamoto, Y. *Rev. Mod. Phys.* **2010**, *82*, 1489−1537.
(6) Carusotto, I.; Ciuti, C. *Rev. Mod. Phys.* **2013**, *85*, 299−366.
(7) Novotny, L. *Am. J. Phys.* **2010**, *78*, 1199−1202.
(8) Törmä, P.; Barnes, W. L. *Rep. Prog. Phys.* **2015**, *78*, No. 013901.
(9) Marquier, F.; Sauvan, C.; Greffet, J.-J. *ACS Photonics* **2017**, *4*, 2091−2101.
(10) Bellessa, J.; Bonnand, C.; Plenet, J. C.; Mugnier, J. *Phys. Rev. Lett.* **2004**, *93*, No. 036404.
(11) Dintinger, J.; Klein, S.; Bustos, F.; Barnes, W. L.; Ebbesen, T. W. *Phys. Rev. B: Condens. Matter Mater. Phys.* **2005**, *71*, No. 035424.
(12) Hakala, T. K.; Toppari, J. J.; Kuzyk, A.; Pettersson, M.; Tikkanen, H.; Kunttu, H.; Törmä, P. *Phys. Rev. Lett.* **2009**, *103*, No. 053602.
(13) Schwartz, T.; Hutchison, J. A.; Genet, C.; Ebbesen, T. W. *Phys. Rev. Lett.* **2011**, *106*, 196405.
(14) Vasa, P.; Wang, W.; Pomraenke, R.; Lammers, M.; Maiuri, M.; Manzoni, C.; Cerullo, G.; Lienau, C. *Nat. Photonics* **2013**, *7*, 128−132.
(15) Chikkaraddy, R.; de Nijs, B.; Benz, F.; Barrow, S. J.; Scherman, O. A.; Rosta, E.; Demetriadou, A.; Fox, P.; Hess, O.; Baumberg, J. J. *Nature* **2016**, *535*, 127−130.
(16) Sanvitto, D.; Kéna-Cohen, S. *Nat. Mater.* **2016**, *15*, 1061−1073.
(17) Orgiu, E.; George, J.; Hutchison, J. A.; Devaux, E.; Dayen, J. F.; Doudin, B.; Stellacci, F.; Genet, C.; Schachenmayer, J.; Genes, C.; Pupillo, G.; Samorì, P.; Ebbesen, T. W. *Nat. Mater.* **2015**, *14*, 1123−1130.
(18) Aberra Guebrou, S.; Symonds, C.; Homeyer, E.; Plenet, J. C.; Gartstein, Y. N.; Agranovich, V. M.; Bellessa, J. *Phys. Rev. Lett.* **2012**, *108*, No. 066401.
(19) Shi, L.; Hakala, T. K.; Rekola, H. T.; Martikainen, J.-P.; Moerland, R. J.; Törmä, P. *Phys. Rev. Lett.* **2014**, *112*, 153002.
(20) Ramezani, M.; Halpin, A.; Fernández-Domínguez, A. I.; Feist, J.; Rodriguez, S. R.-K.; Garcia-Vidal, F. J.; Gómez Rivas, J. *Optica* **2017**, *4*, 31−37.
(21) Hakala, T. K.; Moilanen, A. J.; Väkeväinen, A. I.; Guo, R.; Martikainen, J. P.; Daskalakis, K. S.; Rekola, H. T.; Julku, A.; Törmä, P. *Nat. Phys.* **2018**, *14*, 739−744.
(22) Daskalakis, K. S.; Maier, S.; Murray, R.; Kéna-Cohen, S. *Nat. Mater.* **2014**, *13*, 271−278.
(23) Gómez, D. E.; Vernon, K. C.; Mulvaney, P.; Davis, T. J. *Nano Lett.* **2010**, *10*, 274−278.
(24) Gómez, D. E.; Lo, S. S.; Davis, T. J.; Hartland, G. V. *J. Phys. Chem. B* **2013**, *117*, 4340−4346.
(25) Wang, H.; Wang, H.-Y.; Toma, A.; Yano, T.; Chen, Q.-D.; Xu, H.-L.; Sun, H.-B.; Proietti Zaccaria, R. *J. Phys. Chem. Lett.* **2016**, *7*, 4648−4654.
(26) Santhosh, K.; Bitton, O.; Chuntonov, L.; Haran, G. *Nat. Commun.* **2016**, *7*, 11823.
(27) Liu, W.; Lee, B.; Naylor, C. H.; Ee, H.-S.; Park, J.; Johnson, A. T. C.; Agarwal, R. *Nano Lett.* **2016**, *16*, 1262−1269.
(28) Zakharko, Y.; Graf, A.; Zaumseil, J. *Nano Lett.* **2016**, *16*, 6504−6510.
(29) Zakharko, Y.; Rother, M.; Graf, A.; Hähnlein, B.; Brohmann, M.; Pezoldt, J.; Zaumseil, J. *Nano Lett.* **2018**, *18*, 4927−4933.
(30) Ithurria, S.; Dubertret, B. *J. Am. Chem. Soc.* **2008**, *130*, 16504−16505.
(31) Ithurria, S.; Tessier, M. D.; Mahler, B.; Lobo, R. P. S. M.; Dubertret, B.; Efros, A. L. *Nat. Mater.* **2011**, *10*, 936−941.
(32) Achtstein, A. W.; Antanovich, A.; Prudnikau, A.; Scott, R.; Woggon, U.; Artemyev, M. *J. Phys. Chem. C* **2015**, *119*, 20156−20161.
(33) Yeltik, A.; Delikanli, S.; Olutas, M.; Kelestemur, Y.; Guzelturk, B.; Demir, H. V. *J. Phys. Chem. C* **2015**, *119*, 26768−26775.
(34) Flatten, L. C.; Christodoulou, S.; Patel, R. K.; Buccheri, A.; Coles, D. M.; Reid, B. P. L.; Taylor, R. A.; Moreels, I.; Smith, J. M. *Nano Lett.* **2016**, *16*, 7137−7141.
(35) Salomon, A.; Wang, S.; Hutchison, J. A.; Genet, C.; Ebbesen, T. W. *ChemPhysChem* **2013**, *14*, 1882−1886.
(36) González-Tudela, A.; Huidobro, P. A.; Martín-Moreno, L.; Tejedor, C.; García-Vidal, F. J. *Phys. Rev. Lett.* **2013**, *110*, 126801.

DOI: 10.1021/acs.nanolett.8b03422
Nano Lett. 2019, 19, 108−115

(37) Rossinelli, A. A.; Riedinger, A.; Marqués-Gallego, P.; Knüsel, P. N.; Antolinez, F. V.; Norris, D. J. *Chem. Commun.* **2017**, *53*, 9938−9941.
(38) Chen, O.; Zhao, J.; Chauhan, V. P.; Cui, J.; Wong, C.; Harris, D. K.; Wei, H.; Han, H.-S.; Fukumura, D.; Jain, R. K.; Bawendi, M. G. *Nat. Mater.* **2013**, *12*, 445−451.
(39) Ebbesen, T. W.; Lezec, H. J.; Ghaemi, H. F.; Thio, T.; Wolff, P. A. *Nature* **1998**, *391*, 667−669.
(40) McPeak, K. M.; Jayanti, S. V.; Kress, S. J. P.; Meyer, S.; Iotti, S.; Rossinelli, A.; Norris, D. J. *ACS Photonics* **2015**, *2*, 326−333.
(41) Prins, F.; Kim, D. K.; Cui, J.; De Leo, E.; Spiegel, L. L.; McPeak, K. M.; Norris, D. J. *Nano Lett.* **2017**, *17*, 1319−1325.
(42) Lessel, M.; Bäumchen, O.; Klos, M.; Hähl, H.; Fetzer, R.; Paulus, M.; Seemann, R.; Jacobs, K. *Surf. Interface Anal.* **2015**, *47*, 557−564.
(43) Chervy, T.; Azzini, S.; Lorchat, E.; Wang, S.; Gorodetski, Y.; Hutchison, J. A.; Berciaud, S.; Ebbesen, T. W.; Genet, C. *ACS Photonics* **2018**, *5*, 1281−1287.
(44) Barnes, W. L.; Preist, T.; Kitson, S.; Sambles, J. *Phys. Rev. B: Condens. Matter Mater. Phys.* **1996**, *54*, 6227−6244.
(45) Kitson, S.; Barnes, W. L.; Sambles, J. *Phys. Rev. Lett.* **1996**, *77*, 2670−2673.
(46) van Exter, M. P.; Tenner, V. T.; van Beijnum, F.; de Dood, M. J. A.; van Veldhoven, P. J.; Geluk, E. J.; 't Hooft, G. W. *Opt. Express* **2013**, *21*, 27422−27437.
(47) Guzelturk, B.; Erdem, O.; Olutas, M.; Kelestemur, Y.; Demir, H. V. *ACS Nano* **2014**, *8*, 12524−12533.
(48) Rowland, C. E.; Fedin, I.; Zhang, H.; Gray, S. K.; Govorov, A. O.; Talapin, D. V.; Schaller, R. D. *Nat. Mater.* **2015**, *14*, 484−489.
(49) Eizner, E.; Avayu, O.; Ditcovski, R.; Ellenbogen, T. *Nano Lett.* **2015**, *15*, 6215−6221.
(50) Maier, S. A. *Plasmonics: Fundamentals and Applications*; Springer: Boston, MA, 2007.
(51) Dionne, J. A.; Verhagen, E.; Polman, A.; Atwater, H. A. *Opt. Express* **2008**, *16*, 19001−19017.
(52) Achtstein, A. W.; Scott, R.; Kickhöfel, S.; Jagsch, S. T.; Christodoulou, S.; Bertrand, G. H. V.; Prudnikau, A. V.; Antanovich, A.; Artemyev, M.; Moreels, I.; Schliwa, A.; Woggon, U. *Phys. Rev. Lett.* **2016**, *116*, 1−5.
(53) Diroll, B. T.; Gaulding, E. A.; Kagan, C. R.; Murray, C. B. *Chem. Mater.* **2015**, *27*, 6463−6469.
(54) Fox, M. *Quantum Optics: An Introduction*; Oxford University Press: Oxford, England, 2006.
(55) Scott, R.; Heckmann, J.; Prudnikau, A. V.; Antanovich, A.; Mikhailov, A.; Owschimikow, N.; Artemyev, M.; Climente, J. I.; Woggon, U.; Grosse, N. B.; Achtstein, A. W. *Nat. Nanotechnol.* **2017**, *12*, 1155−1160.
(56) Gao, Y.; Weidman, M. C.; Tisdale, W. A. *Nano Lett.* **2017**, *17*, 3837−3843.

DOI: 10.1021/acs.nanolett.8b03422
Nano Lett. 2019, 19, 108−115